Effects of Electrical and Physical Properties of Barefaced terrain on Backscatter Response

Maurice Ezeoke, Kenneth Tong, Amin Amiri, Allan Al-Armaghany

Abstract—**We investigate the effect of moisture on the dielectric permittivity and surface roughness with backscatter response from four different barefaced terrain. They represent four classes in the Wentworth grain size classification scale. We improve on previous technique used to remotely identify oil sand reservoirs through accurate modeling of the terrain electromagnetic (EM) reflectivity. First we derived the spectroscopic finger print of the four sample classes at high resolution (8cm^{-1}) covering near-infrared and mid-infrared EM regions to investigate the electrochemical bonds present. Then we varied the moisture level of the samples to observe the variation in dielectric permittivity to provide new information on the electrical properties of the sand terrain. Finally development of 3D EM computer models to investigate the complex relationship between barefaced terrain properties with the Radar back scatter response is outlined. The spectroscopic survey observed the reststrahlen effect due to the presence of quartz while calibrated measurements of dielectric response was achieved.**

Keywords—Backscatter, Barefaced terrain, Beach Sand, Computer Simulation, Loamy sand, Wentworth Classification, Dielectric constant

I.   Introduction

The importance of electromagnetic (EM) signal backscatter has been evident since mid-1940 when a covert spy device developed by Léon Theremin was hid in a gift to the U.S ambassador in Moscow. It gathered information undetected from the American embassy for several years using load modulation of acoustic audio [1]. Incident radio frequency (RF) illuminated from across the street caused signals to be reflected from the antenna embedded in the device along with acoustic audio [2]. Since then this principle of Radar backscattering has been applied to a wide number of applications covering communication, networking and remote sensing. For instance backscatter communication based on radar technology is used in the RF identification (RFID) systems applied to logistics, medical and military scenarios while backscatter sensing has been employed in air and spaceborne radar imaging [3].

Interpretation of terrain information derived from radar imaging sensors on satellites, airborne or unmanned aerial vehicle (UAV) platforms depends on the backscatter response. Literature is replete with sensor and terrain parameters that theoretically influence radar backscatter response [4]. Previous investigations involved measurement of the scattering coefficient $\sigma^0(\theta)$, expressed in units of decibels (dB) as a function of incidence angle θ_i. In [5] the like-polarized backscattering coefficients σ^0_{hh} and σ^0_{vv} of three bare farmland soil fields with surface roughness varying from 2 cm to 15 cm were measured as a function of soil moisture content while in [6] measurements were extended to vegetation covered terrain. Both concluded the possibility of monitoring soil moisture content with radar. However the level of sensitivity necessary to achieve this conclusively means that most backscatter research is achieved with radar scatterometers.

Our approach is to develop computer models that reflect the backscattering response obtainable from different barefaced terrain types after determining the physical and electrical properties of the terrain. First physical sizes of the particles are determined using sieve analysis and surface roughness, *S* compared to the grain size particles from the Wentworth scale classification [7]. Next spectroscopic identification of terrain is performed to understand types of electrochemical bonds present. Dielectric properties are investigated in relation to weight percentage wt.%. Initial results provide new information on the relationship between dielectric permittivity and moisture content, m_x (gcm^{-3}). Finally an outline for how the results will be used to develop high resolution EM backscatter simulation models. Section II covers measurements. Section III analyses initial experimental results while IV outlines model development then concludes.

II.   Experimental Measurement

A.   Grain Size

The terrain samples A to D shown in Fig.1 were selected to broadly represent major barefaced terrain particularly beach sand, loamy farm sand, pebbles and granite fragments.

TABLE I.   BARE FACED TERRAIN TYPES

Sample	Name	Size^a
A	Beach Sand	< 0.5
B	Loamy Farm Sand	1-2
C	Pebbles	10
D	Granite	40

a. Wentworth Scale mean particles diameter in mm from [7]

Maurice Ezeoke

Roberts Engineering Building, University College London, WC1E 7JE, UK
uceemse@ucl.ac.uk

B. *Spectral Measurements*

Samples A and B did not require preparation before measurements but C and D were soaked in deionized water and sonicated using a Branson1510 ultrasonic sonicator to extract representative sediments.

(a)	(b)
(c)	(d)
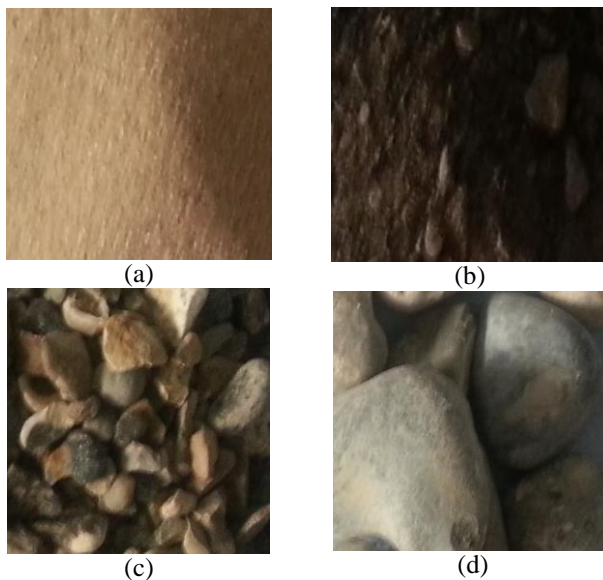
Fig. 1. Barefaced terrain (a) Beach sand (b) Loamy farm sand (c) Pebbles (d) Granite

The sediments were left to settle and then the pebbles and granite were picked off using plastic tweezers taking care not to disturb the sediments. After filtration C and D were placed in foil paper to retain the aromatic residue and mildly heated until all traces of deionized water solvent had evaporated.

The spectral behaviour was investigated with a Shimadzu IRPrestige-21 FTIR 8400S spectrophotometer. The equipment is able to measure reflected thermal energy at wave numbers v, ranging from far infrared (FIR) to near IR (NIR), $v = 12500$ cm^{-1} – 3800 cm^{-1} ($\lambda = 0.8 - 2.63$ μm). The Mid IR (MIR) region covering $v = 4000$ to 400 cm^{-1} ($\lambda = 2.5 - 25\mu$m) was mainly used for the experiment. The beam splitter was changed from potassium bromide to fluorine calcium to examine NIR response.

Minute amounts of each sample were placed one after each other and irradiated with the laser after background measurements were taken to obtain the attenuated total reflectance (ATR) spectra. Two measurements per sample were obtained with the following settings: number of scans, 100; resolution, 8cm^{-1}, gain, auto; range, 4000-400cm^{-1} MIR but 12500-3800cm^{-1} for NIR. Due to variation in the samples there was no need for a control like previous work [3].

C. *Dielectric Measurements*

1) *Definition of Terms*

Precision knowledge of the complex dielectric constant is vital to interpreting the interaction between incident or reflected EM radiation and earth terrain. Terms are defined here for consistency in the constitutive relationships with relevant EM theory equations. The electrical permittivity $\varepsilon^*(\omega)$ and conductivity $\sigma^*(\omega)$ are generally complex, frequency f, dependent parameters that explain the microscopic EM properties of a material. From [8], they are given by:

$$\varepsilon^*(\omega) = \varepsilon'(\omega) - i\varepsilon''(\omega), \tag{1}$$

$$\sigma^*(\omega) = \sigma'(\omega) - i\sigma''(\omega) . \tag{2}$$

From EM theory, the electric flux density D is:

$$\boldsymbol{D} = \varepsilon\boldsymbol{E} \tag{3}$$

Where $\varepsilon \equiv \varepsilon^* \equiv \varepsilon_0\varepsilon_r$ is the absolute permittivity, ε_r is the relative permittivity, $\varepsilon_0 = 8.85 \times 10^{-12}$ *F/m* is the free space permittivity and $\boldsymbol{E}$ is the electric field. The dielectric constant (κ) is given as:

$$\kappa = \varepsilon/\varepsilon_0 = \varepsilon_r = \varepsilon'_r - j\varepsilon''_r \tag{4}$$

The real part of permittivity (ε_r') indicates how much energy from an electric field is stored while the imaginary part (ε_r'') is called the loss factor. It shows how dissipative a material is to an external field. The loss tangent or tan δ shows the ratio of energy lost to that stored i.e. *tan $\delta = \varepsilon''_r / \varepsilon'_r$*.

2) *Experimental Procedure*

The aim was to measure the variation in ε'_r, ε''_r and *tan δ* with m_x of terrain. Several dielectric measurement techniques exist. The developed technique using a coaxial probe with a surface area of 1.5mm^2 is more suitable for materials under test (MUT) with greater contact area for absorption thus only water and samples A and B were measured using this technique.

Samples A and B were heated using a hotplate at a modest temperature (75°C) to remove trace moisture without altering the chemical behaviour. Permittivity of pure terrain sample was obtained and subsequently the weight percentage (wt.%) of moisture and terrain samples was measured using an analytical balance AB304-S Mettler Toledo instrument. Each 10% increase in moisture level of the terrain was balanced by a corresponding decrease in terrain sample to preserve the wt.% balance. For example to create B20W, 80grams of sample B was combined with 20grams (20 millilitres) of water as shown in Fig.2 before mixing occurred. Prior to measurement samples are mixed to create a better combination of terrain and moisture to represent the averaged detail that would be seen in the resolution cell of an EM sensor. Summary of the measurement campaign is shown table 2.

TABLE II.   MEASUREMENT CAMPAIGN

MUT	Test	Remarks
Water	W100-21	100% water at 21°C
Water	W100-C	100% water cold
Beach Sand	A100	100% sample A
Loamy farm	B100	100% sample B
Beach sand: Water	A10W to A50W	Ratio of wt.% increase in water relative to decrease in sample A
Loamy farm sand : Water	B10W to B50W	Ratio of wt.% increase in water relative to decrease in sample B

The dielectric properties were investigated using the Agilent PNA N5227A 10 MHz – 67 GHz network analyser along with an Agilent 85070E dielectric probe kit. Each sample was measured over a range of frequencies covering 0.5 GHz (L-band) through C-band (4-8 GHz) up to 11 GHz (X-band). For each test the equipment were calibrated in air (open), water (load) and short to eliminate systematic measurement errors (Fig. 2). The results from both FTIR and dielectric measurements were processed and analyzed using Matlab software tool [9].
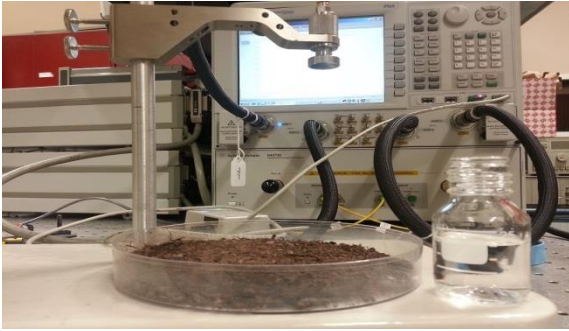
Fig. 2. Generic set up for dielectric measurement of MUT B20W before mixing 80g loamy farm sand and 20g water.

III. Experimental Results

A. Spectral Results

Samples A to D were spectrally characterized. Zoomed-in view of the reflectance spectra covering $v = 750cm^{-1}$ to $3250cm^{-1}$ and $v = 4000 \ cm^{-1}$ to $12000 \ cm^{-1}$ is shown in Fig. 3. Difference in spectral signature is due to the variation in underlying electrochemical bonds. MIR provides greater variation in *% T* peaks (*y* axis) and the spectral location of wavenumber bands (*x* axis) but NIR achieves higher spectral reflectance intensity.
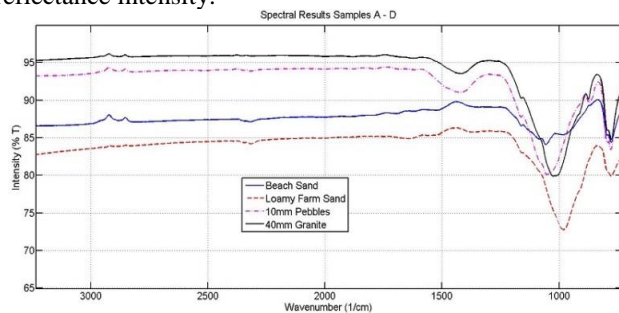
Fig. 3. MIR Reflectance Spectra Samples A-D.

The strong reststrahlen effect witnessed at 1150 cm^{-1} is characteristic of quartz while calcium carbonate (limestone) bands occur near $v = 1400 - 1500 \ cm^{-1}$ [10]. The reststrahlen effect is most evident in A possibly due to larger presence of quartz in the parent substrate or the size of the unprepared grains compared to C and D. Also there is a reduction in *%T* due to limestone presence in C and D compared to A and B.

The similarity in the spectral profiles for C and D is better seen in a normalized plot of the results (Fig. 4). The contrast between C/D and A/B is most evident from 600 to 1200 cm^{-1}.

A is expectedly more reflective than B due to the dominant presence of silicon oxide bonds. However D is more reflective than C due to comparatively greater homogeneity in D.
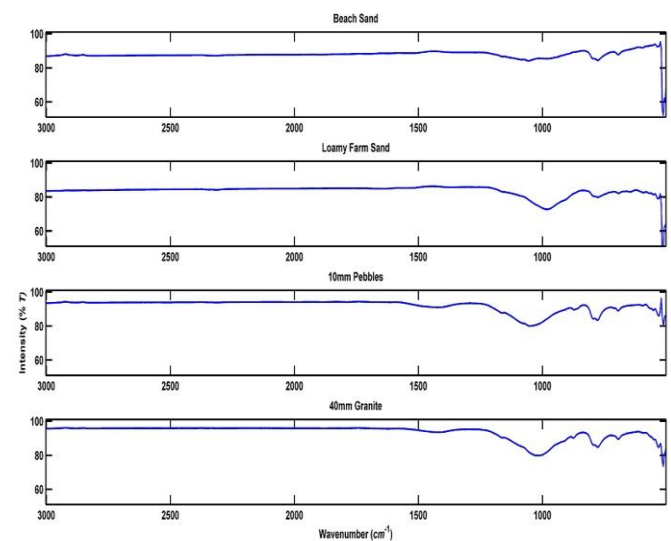
Fig. 4. Normalized Mid IR Transmittance spectra comparing reststrahlen effect at 1150cm^{-1} for Samples A to D

FTIR analysis was used to determine the relative approximate abundances of the mineral bonds present. Glass is an allotrope of silicon and a major constituent in A-D. Summary of major and minor mineral phases is in table 3.

TABLE III.   MAJOR AND MINOR BONDS PRESENT

Sample	Major constituents	Minor constituents
A	Glass, Diatomaceous earth (SiO_2)	Silica-1
B	Glass, NaNO3	Magnesium oxide, MgO, Iron hydroxide, $Fe(OH)_3$
C	Glass, Diatomaceous Earth/Granular $SiO2$, Polystyrene film,	Silica-1, silica-2, glass
D	Glass, SiO_2	Diatomaceous earth/SiO_2, silicon rubber

B. Dielectric Permittivity Results

The dielectric permittivity was measured over frequencies used for radar remote sensing [3]. First we observe that temperature generally has a mild effect on the dielectric behaviour of materials. Cold water (W100-C) resulted in an initially higher ε'_r value at 1GHz. At 8.5GHz the observed ε'_r dropped below W100-21 (Fig.5). W100-21 is also relatively less prone to dissipate EM radiation as frequency increases.

Increase in wt.% of water caused an increase in the measured ε'_r of the terrain. In order to provide a calibrated measurement the wt.% combination of water and terrain was weighed before and after ε'_r values were obtained. The surface roughness initially increased with viscosity forming lumps of terrain particularly sample A (Fig.6). The tipping point occurred after 30 wt.% of water was added to sample A (A30W) but sample B was able to absorb up to 40 wt.%

water without flooding (Fig. 6.d).
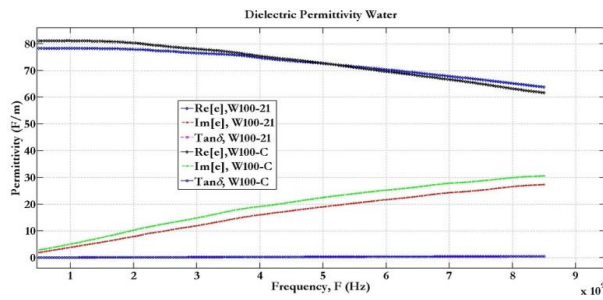
Fig. 5. Temperature effect on permittivity of water

A section of the average ε'_r values obtained with increasing m_x is shown in table 5. The ε'_r value of water is 30 times the value of dry terrain while the ε''_r is over 100 times larger. This is why terrain moisture level causes an appreciable effect in the backscattering response. We observed experimental errors in the region of 2.5% due to variation in the probe position mostly during early stages when the wt% of water was lowest (A10W and B10W). Results of measurements of the real permittivity and loss factor are presented in Fig.7.

IV. **Conclusion**

Three major trends observed include: (a) the reduction in ε'_r with f regardless of the amount of water present (b) real ε'_r increased with m_x and (c) reduction in ε''_r from 1-2 GHz but subsequent increases. Importantly there is a Kramers-Krönig correlation between ε'_r and ε''_r because the real component of the response at each f is related to the imaginary part.

The 3D models will be based previous simulation technique with generic configuration developed in [3]. However the results of the dielectric measurement will cause extensive improvements to the range and quality of the initial datasets. The processing mechanism will be updated to cope with the large amount of data generated. In total we envisage 56 models to be developed with each data set comprising 218 values of scattering coefficient, σ^0 corresponding to combinations of sensor and terrain parameters. The main simulation parameters are shown in table 4. Three aspects of the EM reflectivity will be considered. These will be the radar cross section (RCS), the absorption cross section (ACS) and EM scattering field within a resolution.

TABLE IV.   SIMULATION PARAMETERS TO BE USED IN MODEL

Parameter	Value
Incidence angle, θ_i	90°, 60°, 55°, 45°, 35°, 30°, 20°
Freq. band (GHz)	L- (1), C- (5), X- (10)
Resolution cell, dA	1 m³
Sensor position (m)	5, 1, 0.5, 0, -0.1, -0.5

References

[1] A. Glinsky, *Theremin: Ether Music and Espionage.* Champaign, IL: Univ. Illinois Press, 2000, pp.119-122.

[2] H. Stockman, "Communication by means of reflected power," *Proc. IRE,* vol. 36, no.10, pp. 1196-1204, 1948.

[3] M. Ezeoke and K. Tong, "Modeling electromagnetic reflectivity of Agbabu Oil Sand from Hyperspectral Infrared Reflectance Spectra and Dielectric Properties at L-, C- and X-band Frequencies", *proceedings of IEEE 5th Computational Intelligence, Communication Systems and Networks* (CICSyN 2013), 5-7 June, 2013, pp 125-130..

[4] T.M. Lillesand, R.W. Kiefer, J.W. Chipman, *Remote Sensing and Image Interpretation*, 5th Ed, Madison, WI: John Wiley & Sons, 2004, pp.763.

[5] F.T. Ulaby, P.P. Batlivala, and M.C.Dobson, "Microwave backscatter dependence on surface roughness, soil moisture and soil texture, Part I: Bare soil," *IEEE Trans. Geosci. Electron.,* Vol. GE-16, Oct. 1978, pp.286-295.

[6] F.T. Ulaby, G.A. Bradley, and M.C.Dobson, "Microwave backscatter dependence on surface roughness, soil moisture and soil texture, Part II: Vegetation-covered soil," *IEEE Trans. Geosci. Electron.,* Vol. GE-17, No. 2, April 1979, pp. 33-40.

[7] C.K. Wentworth, "A scale of grade and class terms for clastic sediments", *Journal of Geo.,* Vol. 31, 1922, pp.228-232.

[8] S.H. Ward, and G.W. Hohmann, Electromagnetic theory for geophysical applications, in *Electromagnetic Methods in Applied Geophysics*, edited by M.N. Nabighian, pp. 130-311, Soc. Of Explor. Geophys., Tulsa, Okla., 1988.

[9] Matlab www.mathworks.co.uk

[10] R.R. Willey, "Emittance and reflectance of various materials in the 2 to 20 micrometer spectral region", *SPIE,* vol. 643 Infrared, Adaptive and Synthetic Aperture Optical Systems, 1986.

About Author (s):

"Improve on previous technique used to remotely identify oil sand reservoirs". Maurice obtained MSc with distinction from Surrey. His PhD research at UCL uses radar to prospect unconventional petroleum resources.

Kenneth received B.Eng. (Hons.) and Ph.D. degrees in Engineering from City University of Hong Kong. He is interested in the "interaction between EM waves and matter" and has built innovative antennas for niche uses.

"Dielectric permittivity influences propagation effects of radar signal in terrain". Amin's PhD research at UCL focusses on the detection of landmines and IEDs using ground penetrating radar from UAVs.

Allan graduated with a first class degree from UCL. His PhD research at UCL develops non-contact microwave monitor for cancer treatment based on nuanced differences in blood conductivity and permittivity.
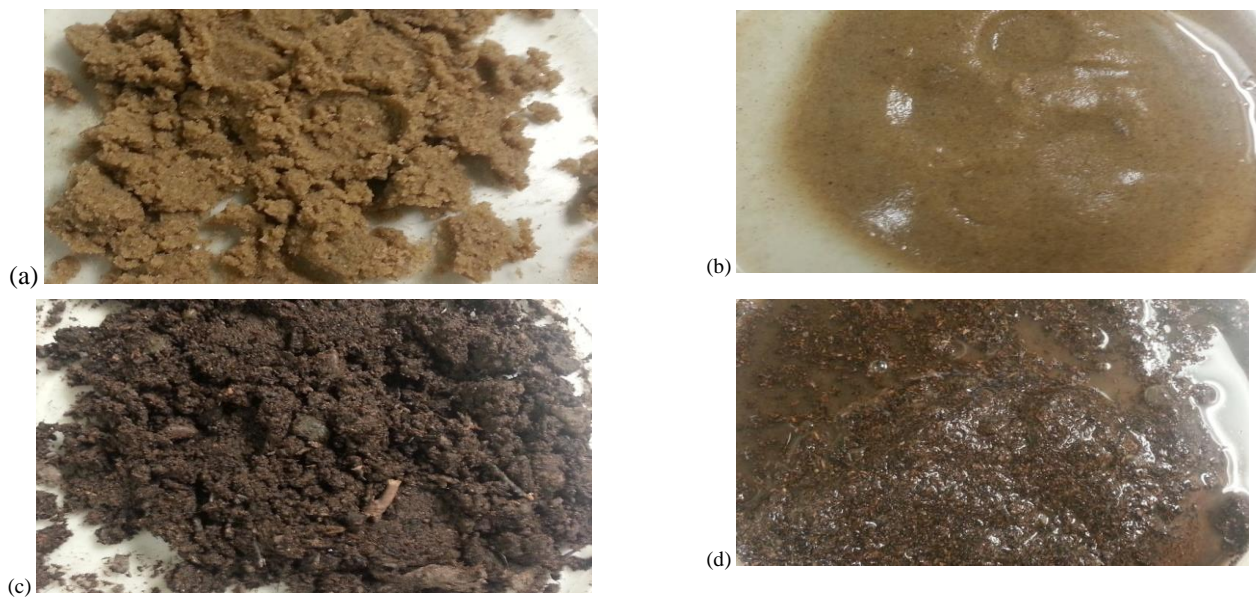
Fig. 6. Increasing wt.% of water. (a) A20W (b) A30W (c) B30W (d) B50W

TABLE V.　　SOME RESULTS OF REAL PERMITTIVITY MEASUREMENTS AT ROOM TEMPERATURE

f (GHz)	Real Permittivity, ε'_r											
	A100	**B100**	**A10W**[b]	**B10W**	**A20W**	**B20W**	**A30W**	**B30W**	**A40W**	**B40W**	**A50W**	**B50W**
1.03	2.54	1.57	7.02	5.03	17.08	7.57	27.54	17.48	27.69	30.62	27.55	30.72
5.00	2.53	1.54	6.23	4.24	14.73	6.52	23.81	14.65	24.03	25.30	23.87	25.40
7.05	2.47	1.52	6.23	4.20	14.62	6.50	23.27	14.47	23.63	24.40	23.54	24.52
8.50	2.41	1.50	6.38	4.26	14.67	6.61	23.09	14.52	23.55	24.26	23.50	24.47

b. A[N]W refers to a mixture of (100 – N) wt.% of Sample A and N wt.% of water.
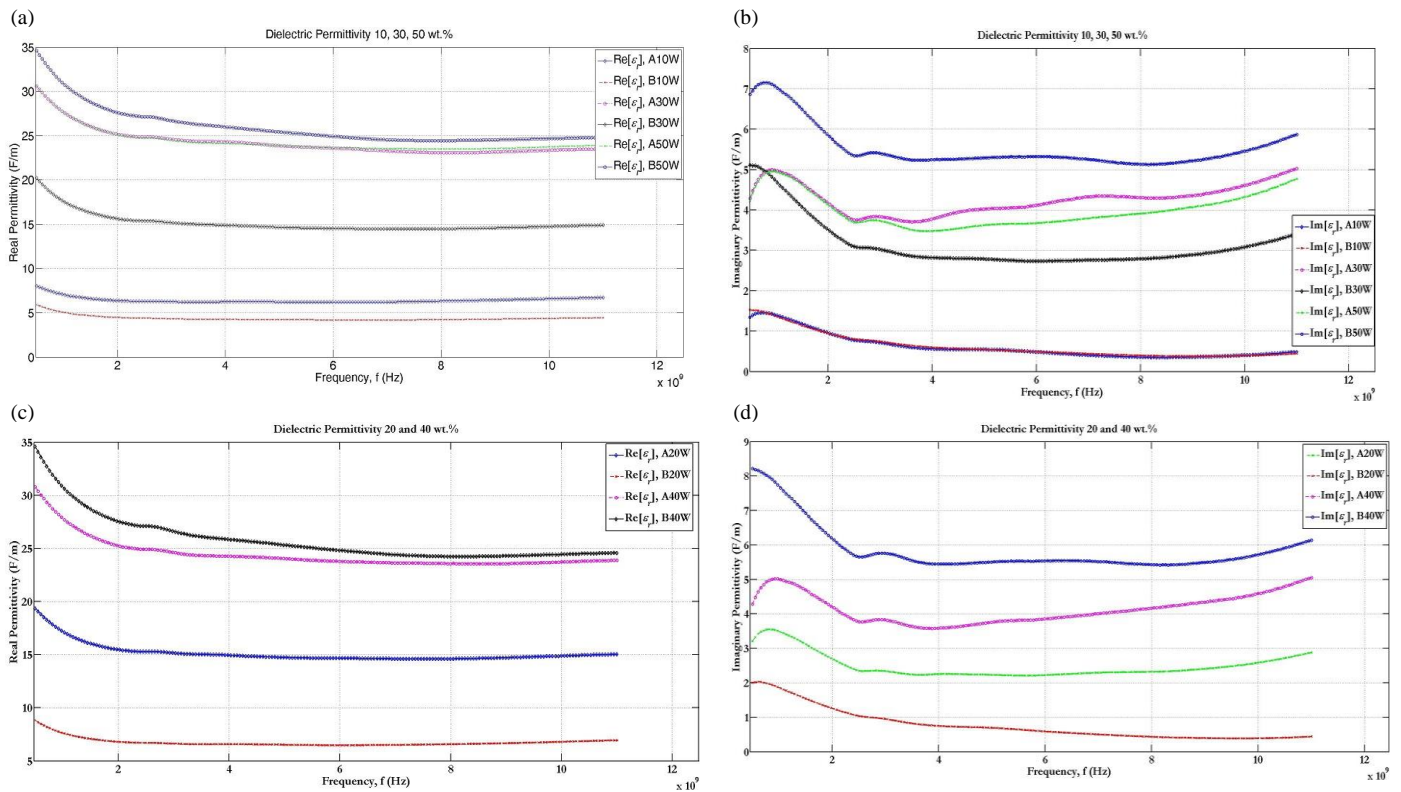
Fig. 7. Permittivity variation with increasing wt.% of water. (a) ε_r' and (b) ε_r'' for 10, 30, 50 wt.% (c) ε_r' and (d) ε_r'' for 20 and 40 wt.%